PG
Petroleum Geoscience

Research article

Published Online First

https://doi.org/10.1144/petgeo2016-162

South China Sea crustal thickness and oceanic lithosphere distribution from satellite gravity inversion

Simon Gozzard[1,2*], Nick Kusznir[1], Dieter Franke[3], Andrew Cullen[4,5], Paul Reemst[4] & Gijs Henstra[4]

[1] Department of Earth, Ocean and Ecological Sciences, University of Liverpool, 4 Brownlow Street, Liverpool L69 3BX, UK
[2] Shell International Ltd, 40 Bank Street, London E14 5NR, UK
[3] Federal Institute for Geosciences and Natural Resources, Stilleweg 2, 30655 Hannover, Germany
[4] Shell International Exploration and Production, Carel van Bylandtlaan 16, NL 2501, The Hague, The Netherlands
[5] Chesapeake Energy, Oklahoma City, OK 73118, USA

D.F., 0000-0002-1488-026X; P.R., 0000-0002-2443-9902; G.H., 0000-0001-9805-5875

*Correspondence: s.gozzard@shell.com

Abstract: Inversion of satellite-derived free-air gravity-anomaly data has been used to map crustal thickness and continental lithosphere thinning in the South China Sea. Using this, we determine the ocean–continent transition zone structure, the distal extent of continental crust, and the distribution of oceanic lithosphere and continental fragments in the South China Sea. We construct a set of regional crustal cross-sections, with Moho depth from gravity inversion, spanning the South China Sea from offshore China and Vietnam to offshore Malaysia, Brunei and the Philippines to examine variations in ocean–continent transition structure and ocean-basin width. Our analysis shows a highly asymmetrical conjugate margin structure. The Palawan margin shows a narrow transition from continental to oceanic crust. In contrast, the conjugate northern margin of the South China Sea shows a wide region of thinned continental crust and an isolated block of continental crust (the Macclesfield Bank) separated from the Chinese margin by a failed oceanic rift. The Dangerous Grounds are predicted to be underlain by fragmented blocks of thinned continental crust. We use maps of crustal thickness and continental lithosphere thinning from gravity inversion together with free-air gravity- and magnetic-anomaly data to identify structural trends and to show that rifting and the early seafloor-spreading axis had an ENE–WSW trend while the later seafloor-spreading axis had a NE–SW trend.

Received 19 December 2016; **revised** 2 January 2018; **accepted** 11 February 2018

The distribution of oceanic crust and lithosphere within the South China Sea (SCS) are controversial. Knowledge of ocean–continent transition zone (OCTZ) structure and the distal extent of continental crust are of critical importance to deep-water frontier play evaluations in hydrocarbon exploration. In this paper, we use 3D gravity-anomaly inversion to map Moho depth, crustal thickness and continental lithosphere thinning for the SCS in order to determine OCTZ structure, the distal extent of continental crust and the distribution of oceanic lithosphere. The gravity-inversion method incorporates a lithosphere thermal gravity-anomaly correction which for much of the SCS exceeds −100 mgal in magnitude because of the young formation age of the SCS. Regional 3D mapping of SCS crustal thickness and oceanic lithosphere distribution is supplemented by crustal cross-sections with Moho depth from gravity inversion to give insights into OCTZ structure and its along-strike variations. Gravity-inversion predictions of Moho depth and continental lithosphere thinning factor determined using regional public-domain sediment-thickness data are compared with those determined using sediment thickness for a regional seismic profile spanning the SCS; their comparison providing corroboration of the techniques and data used.

The distribution of oceanic lithosphere within the SCS and the structure of its OCTZ have been the focus of many investigation in recent decades (e.g. Taylor & Hayes 1980; Pigott & Ru 1994; Sun *et al.* 2009; Franke *et al.* 2011; Expedition 349 Scientists 2014; Gao *et al.* 2016; Ding & Li 2016; Cameselle *et al.* 2017; Wan *et al.* 2017). As these investigations have proceeded, our understanding of the complexity of rifted continental margin formation processes and OCTZ structure has also progressed. Our present understanding of OCTZ structure at magma-poor rifted margins suggests five zones (Mohn *et al.* 2012; Tugend *et al.* 2014). Running from continent to ocean, these zones are: (i) continental crust of original thickness with only minor rifting; (ii) the necking region where continental crust thins from full thickness down to *c.* 10 km; (iii) hyper-extended continental crust with thickness <10 km; (iv) serpentized exhumed mantle (often with small fragments of continental crust); and (v) oceanic crust generated by seafloor spreading with steady-state decompression melting. For margins with normal or magma-rich decompression melting, the zones of mantle exhumation and hyper-extended continental crust may be absent. Identifying and distinguishing these different zones using gravity inversion alone is not possible. Oceanic crust may have thicknesses similar to those of hyper-extended continental crust. Serpentinized mantle has a gravity-anomaly expression similar to that of 3 km-thick crust (Cowie *et al.* 2015) and so is indistinguishable from thin oceanic crust or extremely hyper-extended continental crust. Nonetheless, crustal-thickness mapping using gravity inversion provides a useful regional constraint on the distribution of continental and oceanic crust, and OCTZ structure.

The SCS presents an opportunity to investigate the recent formation of an ocean basin and its continental margins (Fig. 1). Much of our existing understanding of continental rifted margin formation during continental break-up is derived from seismic experiments and scientific drilling along the continental margins of the Atlantic Ocean. These margins are mature, typically of Jurassic or Cretaceous–Early Cenozoic age, and often covered by significant accumulations of sediment impeding our observations of the OCTZ. Although SE Asia has the highest terrigenous inputs in the world (Milliman & Meade 1983), rapid subsidence in the basins adjacent to the SCS has largely captured this sediment, leading to a relatively

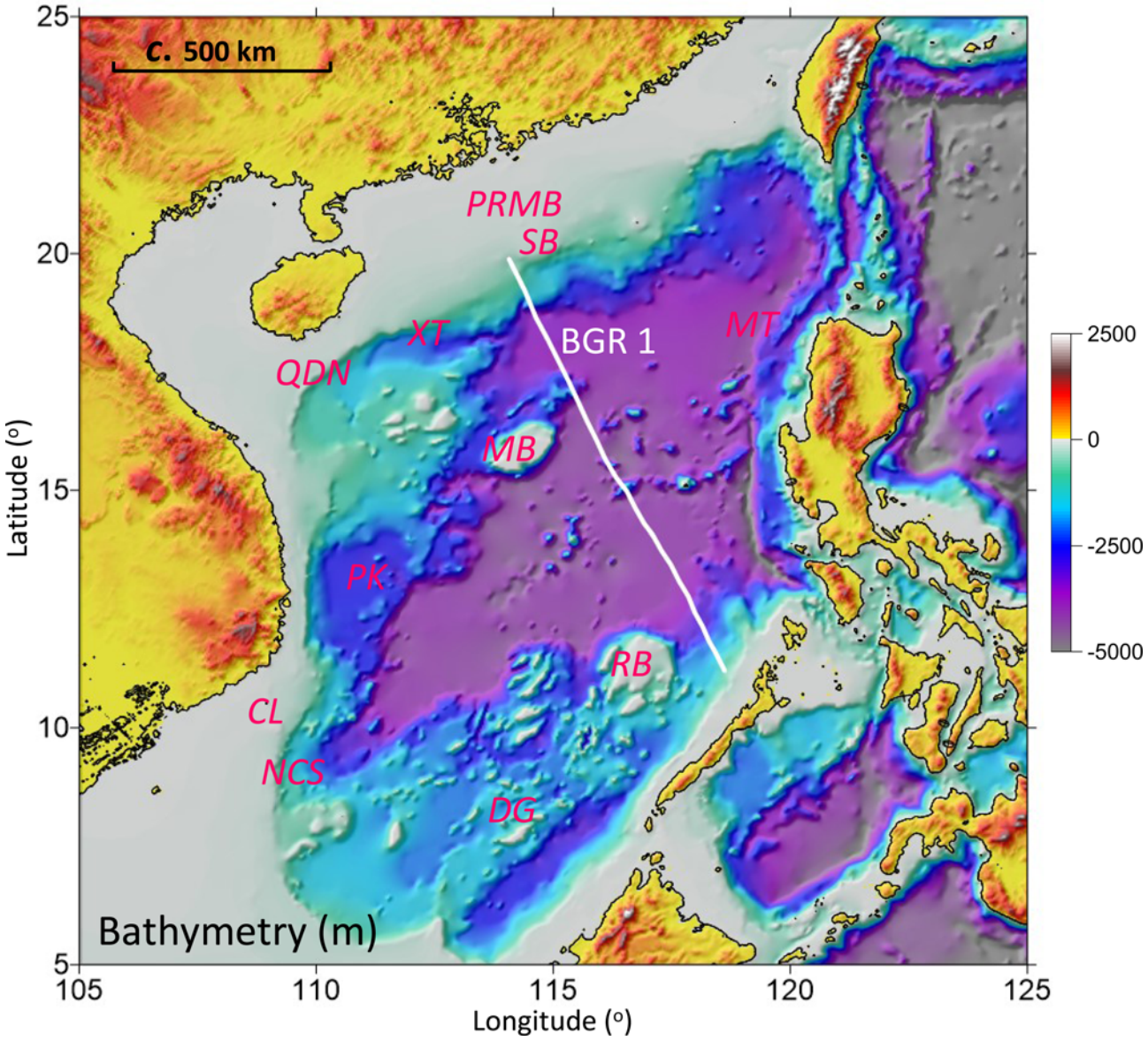

Fig. 1. Regional bathymetry showing the location of seismic line 1 and features referenced in the text: MB, Macclesfield Bank; MT, Manila Trench; PRMB, Pearl River Mouth Basin; RB, Reed Bank; SB, Shuangfeng Basin; XT, Xisha Trough. See the text for data sources.

thin sedimentary cover at the OCTZ of the SCS. This thin sediment cover, coupled with geological and geophysical constraints from industry and ODP/IODP drilling, creates the opportunity for detailed studies of the formation of the SCS ocean basin and its conjugate rifted continental margins (Clift *et al.* 2002; Franke *et al.* 2014; Liu *et al.* 2014; McIntosh *et al.* 2014; Pichot *et al.* 2014; Zhao *et al.* 2016).

Geological formation and setting

Seafloor spreading and the formation of oceanic crust in the SCS, based on the interpretation of ocean-floor magnetic anomalies, started in the Early Oligocene at *c.* 33 Ma and continued until as late as Early–Middle Miocene (Briais *et al.* 1993; Barckhausen & Roeser 2004; Barckhausen *et al.* 2014). Recently, basalts cored during ODP Expedition 39 near the extinct ridge axis yielded Ar/Ar ages of between 17.9 and 14.97 Ma (Koppers 2014).

Continental lithospheric rifting and thinning, prior to continental break-up and initiation of seafloor spreading at *c.* 33 Ma, started with initial uplift of the rift shoulders and widespread erosion in the latest Cretaceous–Early Paleocene (Taylor & Hayes 1980; Pigott & Ru 1994; Schlüter *et al.* 1996). Rifting appears to have occurred in several episodes. Fault analysis along the northern conjugate margin of the SCS in the Pearl River Mouth Basin suggests at least two episodes of rifting (Pigott & Ru 1994). The earlier Cretaceous–Paleocene rift episode resulted in NE–SW-orientated extensional faults. The second Late Eocene–Early Oligocene rift episode is expressed as east–west-orientated normal faults. Regional volcanic activity is associated with a third episode of rifting in the Middle Miocene (Pigott & Ru 1994; Zhao *et al.* 2016) after seafloor spreading had stopped.

During the Paleogene, Reed Bank, on the southern SCS margin, was still attached to the South China continent and was probably joined to the Macclesfield Bank. Continental crustal basement rocks dredged from fault scarps in the Spratly Islands (Kudrass *et al.* 1985; Hutchison & Vijayan 2010) suggests that the region NW of Palawan is a continental block that separated from mainland Asia during the opening of the SCS. This interpretation is similar to that of Franke *et al.* (2008), who interpreted margin-parallel rift basins in continental crust on the NW Palawan shelf. The Manila Trench is a distinct bathymetric feature from about 20° N to about 13° N at which oceanic lithosphere of the SCS is presently being subducted (Fig. 1). East of the Manila Trench, the Philippines consist of an assemblage of terranes of uncertain origin (Hall 2002) and the

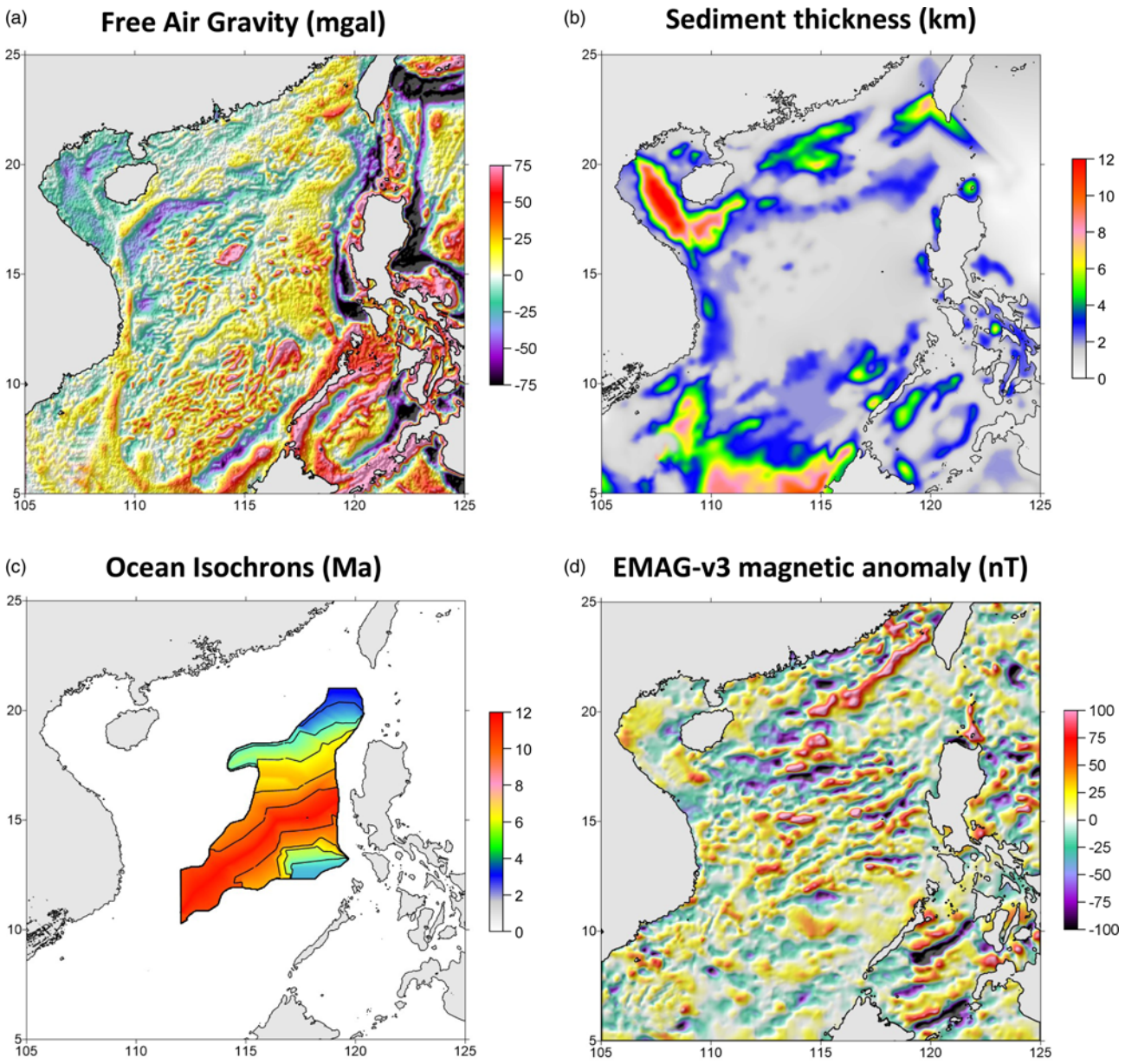

Fig. 2. Data used in the gravity inversion in addition to bathymetry. (**a**) Free-air gravity anomaly with superimposed shaded relief of itself. (**b**) Sediment thickness. (**c**) Ocean isochrons. (**d**) EMAG2-v3 magnetic anomaly with superimposed shaded relief of itself. See the text for data sources.

extent of continental crust having a mainland Asia affinity is not established. Definite continental crust material is found on the islands of Mindoro (Mitchell & Leach 1991), northern Palawan and Panay (Gabo *et al.* 2009). Recently, it has been speculated that portions of the West Luzon shelf are underlain by continental fragments that support rifting prior to and during the opening of the SCS (Arfai *et al.* 2011). In the Middle–Late Cenozoic these continental fragments, including the Dangerous Grounds, collided with an earlier subduction zone either along the Cagayan Ridge in the Sulu Sea (Hinz *et al.* 1994) or with the Philippine Arc further east (Yumul *et al.* 2009).

Crustal thickness and continental lithosphere thinning determined from gravity inversion using public-domain data incorporating a lithospheric thermal gravity-anomaly correction

Gravity-inversion methodology

Gravity inversion of satellite free-air gravity-anomaly data, incorporating a lithospheric thermal gravity-anomaly correction, has been used to determine Moho depth, crystalline crustal thickness and continental lithosphere thinning ($1-1/\beta$) for the SCS and surrounding area. The global coverage of satellite-derived gravity data offers a good basis to undertake large-scale studies of regional crustal structure. The elevated lithosphere geotherm of the young oceanic and rifted continental margin lithosphere of the SCS produces a significant lithosphere thermal gravity anomaly; for active seafloor spreading, this lithosphere thermal gravity anomaly can be as large as −350 mGal. For the SCS, the magnitude of the present-day lithosphere thermal gravity anomaly is well in excess of −100 mgal. Failure to include a correction for the lithosphere thermal gravity anomaly leads to a substantial overestimate of Moho depth and crystalline crustal thickness, and an underestimate of continental lithosphere thinning. A correction is therefore required for this lithosphere thermal gravity anomaly in order to determine Moho depth and crustal thickness accurately from gravity inversion.

The gravity-inversion methodology incorporating a lithosphere thermal gravity-anomaly correction is described in detail by Greenhalgh & Kusznir (2007), Chappell & Kusznir (2008) and Alvey *et al.* (2008). In summary, the observed satellite free-air gravity is first corrected for the gravity contributions of bathymetry

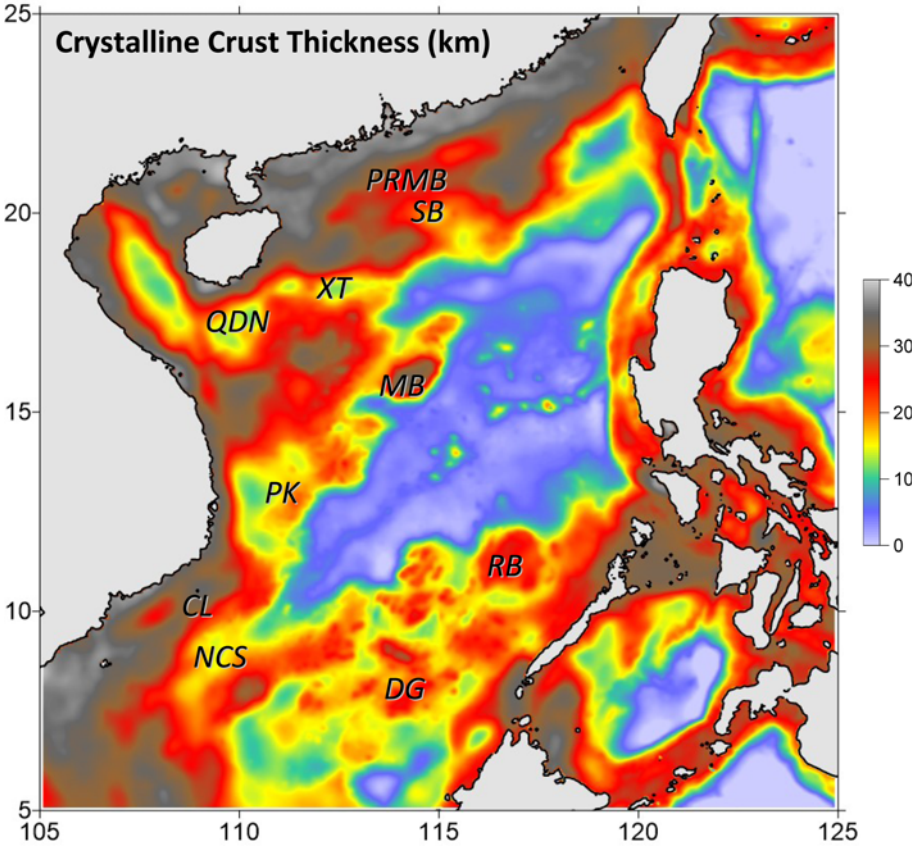

Fig. 3. Crystalline crustal thickness predicted by gravity inversion incorporating a lithosphere thermal gravity-anomaly correction for the South China Sea and adjacent margins.

and sediments (assuming a compaction-controlled sediment density–depth relationship). These data are then filtered to remove short wavelength components (using a Butterworth filter with a 100 km wavelength cut-off). The remaining gravity anomaly is then inverted in the 3D spectral domain using the technique of Parker (1972) to give 3D Moho relief and depth with respect to sea level. From the depth of this 3D Moho surface, the thickness of crystalline crust is then calculated by subtracting water depth (or adding elevation on land) and sediment thickness.

The thinning of continental crustal thickness and lithosphere – defined as $(1-1/\beta)$, where β is the stretching factor – determined from gravity inversion is used to calculate the present-day 3D lithosphere thermal anomaly, which in turn is used to calculate the lithosphere thermal gravity-anomaly correction. The present-day thermal anomaly is calculated using a 3D lithosphere thermal model based on the McKenzie (1978) model of continental lithosphere stretching and thinning. The initial perturbation of the geotherm within the oceanic and rifted continental margin lithosphere is defined by the thinning factor $(1-1/\beta)$, calculated from the crystalline crustal thickness determined from gravity inversion referenced to the initial crustal thickness (assumed in this region to be 37.5 km). For continental margin lithosphere, the thermal equilibration (cooling) time of the lithosphere thermal model is set to the break-up age. For oceanic lithosphere, ocean isochrons are used to give the cooling time, provided that they are reliable. Lithosphere thinning for both continental and oceanic lithosphere is determined solely from the gravity inversion. The methodology by which the thermal gravity-anomaly correction is included in the gravity inversion is described in detail in Alvey *et al.* (2008) and Chappell & Kusznir (2008) .

The continental lithosphere thinning factor ranges from 0 to 1. A thinning factor of 0 corresponds to no stretching and thinning of continental crust and lithosphere, while a value of 1 indicates no continental crust or lithosphere remains. Thinning factors of 1 therefore correspond to oceanic crust or possibly exhumed mantle (see Cowie *et al.* 2015 for a further discussion). Regions with thinning between 1 and 0.7 correspond to a mixture of thinned continental crust and magmatic material.

Stretching and thinning of continental lithosphere thins the continental crust but, as thinning increases, generates new magmatic crust by decompression melting, eventually forming oceanic crust. A correction for the formation of new crust by decompression melting is included in the calculation of continental lithosphere thinning, and uses a parameterization of the model of White & McKenzie (1989). For normal decompression melting, this produces an oceanic crust *c.* 7 km thick (see Chappell & Kusznir 2008 for a more detailed discussion). By subtracting the predicted magmatic addition from the total crystalline crustal thickness predicted by gravity inversion, the residual thickness of continental crystalline crust may be calculated.

The data used in the gravity inversion to determine Moho depth are shown in Figures 1 and 2, and consists of bathymetry (Smith & Sandwell 1997 and updates), free-air gravity anomaly (Sandwell & Smith 1997 and updates), NOAA-NGDC sediment thickness (Divins 2003) and ocean age (Barckhausen & Roeser 2004; Barckhausen *et al.* 2014).

Crustal thickness in the SCS

The resulting maps of crystalline crustal thickness, Moho depth, continental lithosphere thinning and residual continental crystalline crustal thickness for the SCS predicted by gravity inversion are shown in Figures 3 and 4. Continental lithosphere thinning and residual continental crystalline crustal thickness have been calculated, unless otherwise stated, assuming a decompression melting parameterization that generates oceanic crust of normal thickness (i.e. 7 km).

The map of crystalline crustal thickness (Fig. 3) shows a region of very thin crust, with a thickness of 7 km or less in the central SCS. We interpret areas with a crustal thickness of 7 km or less as oceanic

crust; however, we do not exclude that some of this area may contain a mixture of continental fragments and magmatic material, or exhumed mantle material. In the interpreted oceanic portions of the SCS, Moho is predicted to have a depth of about 10–12 km (Fig. 4a). The regions with thinning factors of 1 (or almost 1) (shown in Fig. 4b) indicate the likely distribution of oceanic crust for the SCS.

A thickness of 10 km has been proposed to correspond to the transition from necked continental crust to hyper-extended continental crust (Tugend *et al.* 2014; Cowie *et al.* 2015). Crust between *c.* 7 and 10 km in thickness may be hyper-extended continental crust, thick oceanic crust or a mixture of both. We interpret crust with thickness of 10 km or more as necking zone and proximal continental crust, with the exception of the seamounts along the fossil ocean ridge axis of the SCS. To the north on the South China margin, the predicted crustal thickness and Moho depth (Figs 3 and 4a) increase northwards to *c.* 35 km. In contrast, beneath the Dangerous Grounds the crustal thickness and Moho depth are less, being between 10 and 30 km and 15–30 km, respectively. Between the inferred oceanic crust and original thickness continental crust (>30 km) there are complex domains of thinned continental crust. Both the Read Bank and the Macclesfield Bank, together with other banks, show relatively less thinning. Between these banks there are potential fragments of highly thinned continental crust mixed with magmatic material.

Crust of thickness 10–15 km, corresponding to necked continental crust, is predicted to extend westwards from oceanic crust north of the Macclesfield Bank via the Xisha Trough into the Quiondongnan (QDN) Basin and is interpreted as being generated by stretching and thinning of continental lithosphere ahead of westwards-propagating seafloor spreading, most probably in the Oligocene. Further south, thin crust is predicted in the Phu Khanh Basin. Under the Nam Con Son and Cuu Long basins, offshore southern Vietnam, thinned continental crust is predicted; for the Nam Con Son Basin, crustal thickness ranges between 10 and 15 km. This basin formed ahead of the propagating tip of seafloor spreading, presumably of Miocene age.

The distribution of residual crystalline continental crust thickness within the OCTZ after rift and break-up stretching and thinning is shown in Figure 4c. The mapping of the thickness of residual continental crust is important for heat-flow prediction and petroleum systems modelling because this crust contains radiogenic heat productivity.

Sensitivity tests of the gravity-inversion results

The lithosphere thermal gravity-anomaly correction used in the gravity inversion is sensitive to the thermal re-equilibration time (cooling time) of the lithosphere. The thermal correction has the effect of shallowing the Moho calculated from the gravity inversion, which reduces the predicted crustal thickness and increases the lithosphere thinning factor. For the preferred general gravity-inversion model illustrated in Figures 3, 4 and 5a and b, we assume a cooling time for oceanic lithosphere given by the ocean age isochrons of Barckhausen *et al.* (2014). For all other lithosphere, the cooling time is set to 33 Ma, corresponding to the time of Oligocene continental break-up in the eastern part of the SCS. The sensitivity to the lithosphere thermal cooling times is shown in Figure 5. The effect of using a younger continental break-up age of 20 Ma, more applicable to the SCS in the SW, is shown in Figure 5c and d. The result of reducing the lithosphere cooling time from 33 to 20 Ma for regions not covered by the Barckhausen *et al.* (2014) isochrons is to increase the present-day lithosphere thermal anomaly and, therefore, the magnitude of the lithosphere thermal gravity-anomaly correction. This results in a slightly thinner crust and larger thinning factor; however, the difference is small as seen by a comparison of

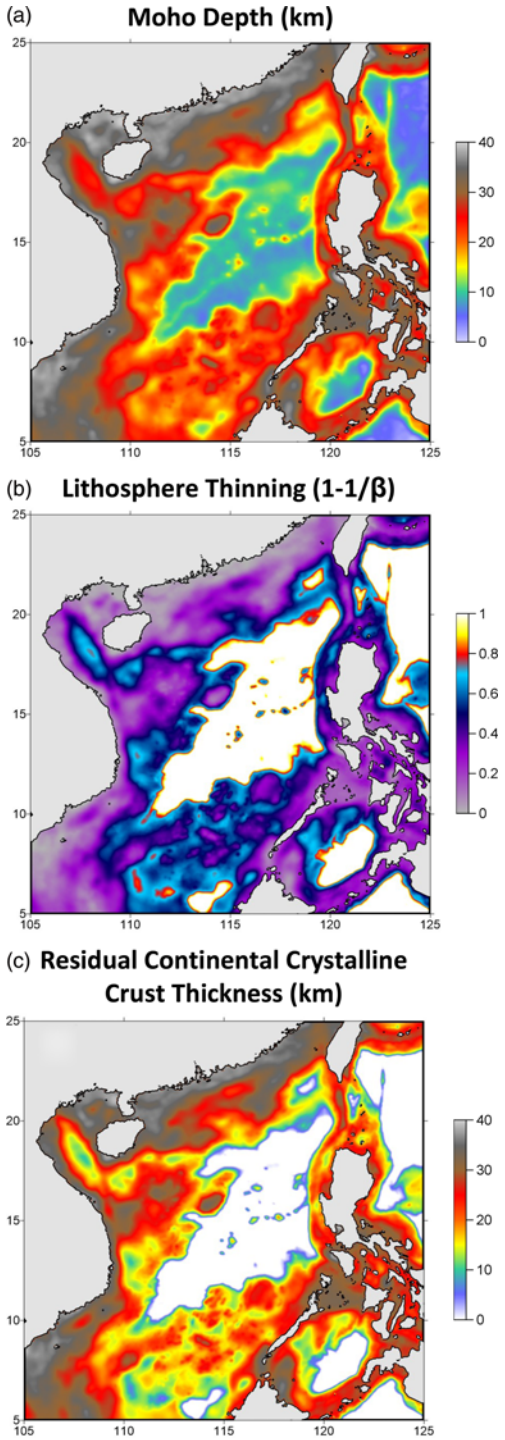

Fig. 4. (**a**) Moho depth. (**b**) Continental lithosphere thinning (1−1/β). (**c**) Residual continental crystalline crustal thickness predicted by gravity inversion incorporating a lithosphere thermal gravity-anomaly correction for the South China Sea and adjacent margins.

Figures 5a and b with Figure 5c and d. The consequence of not using ocean isochrons to determine the cooling time of oceanic lithosphere and instead using a break-up age of 33 Ma for the cooling time of all lithosphere is shown in Figure 5e and f. This homogeneous older age for initial seafloor spreading results in greater cooling of the lithosphere in the western SCS, particularly within oceanic regions, a decrease in the lithosphere thermal gravity-anomaly correction, and consequently a deeper Moho, a thicker crust and a lower thinning factor.

Notwithstanding these sensitivities to lithosphere cooling times, the predicted pattern of crustal thickness and lithosphere thinning,

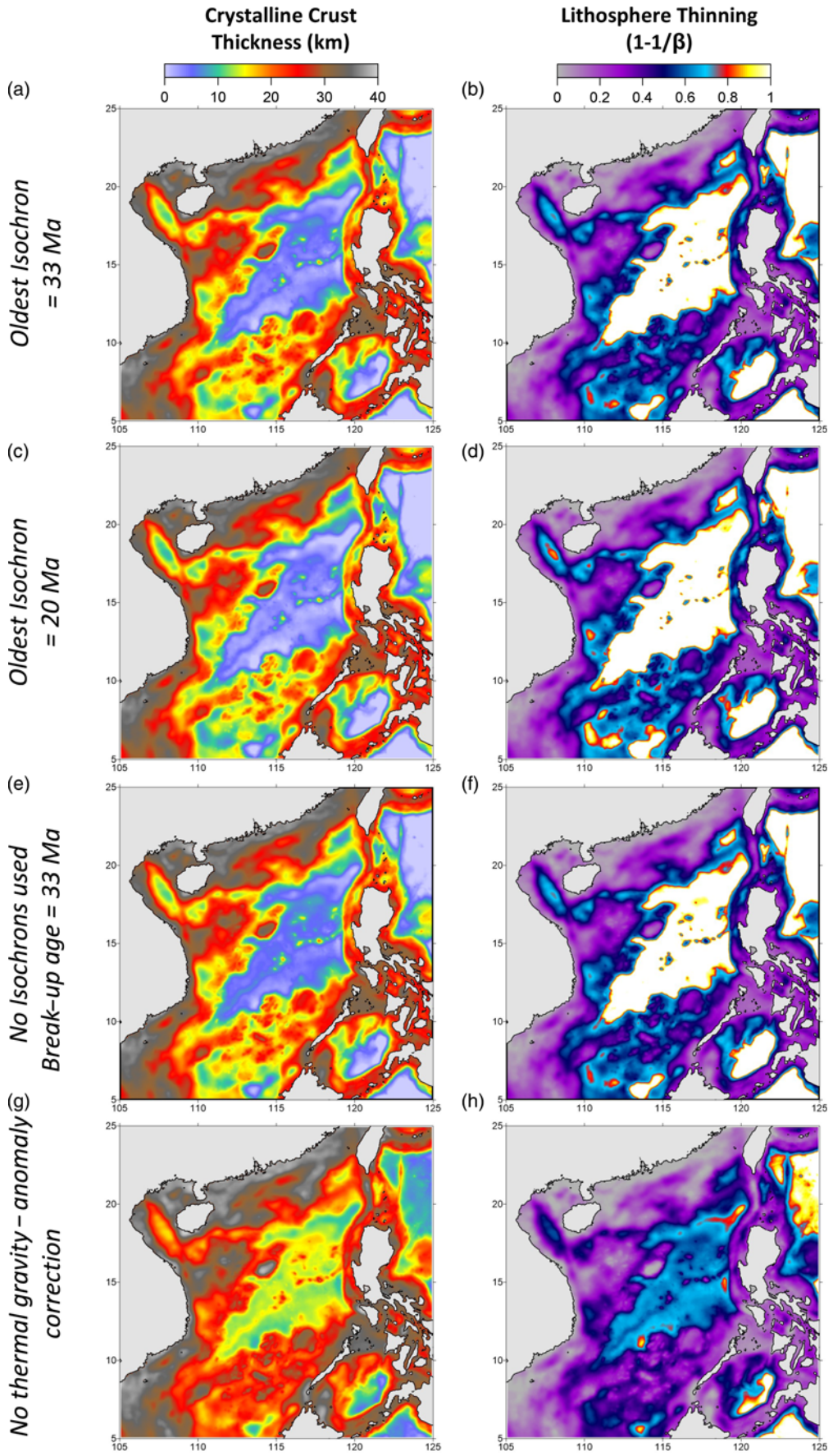

Fig. 5. Crustal thickness and continental lithosphere thinning (1−1/β) determined from gravity inversion showing sensitivity to ocean isochron and break-up ages used to determine the lithosphere thermal gravity-anomaly correction. (**a**) & (**b**) Using oldest isochron and break-up age = 35 Ma. (**c**) & (**d**) Using oldest isochron and break-up age = 20 Ma. (**e**) & (**f**) No isochrons used, break-up age = 35 Ma. (**g**) & (**h**) No lithosphere thermal gravity-anomaly correction used.

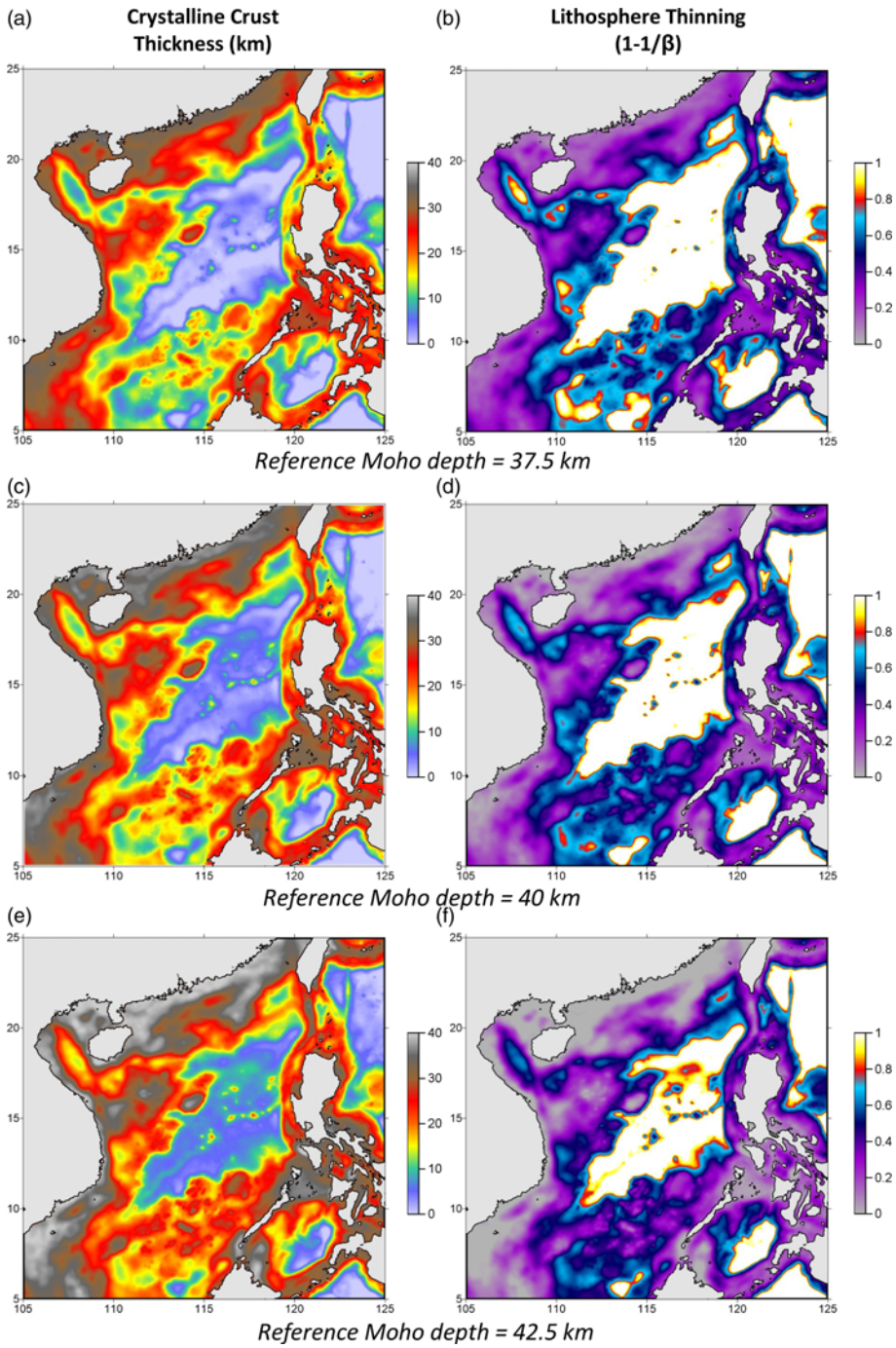

Fig. 6. Sensitivity of crustal thickness and continental lithosphere thinning determined from gravity inversion to reference Moho depth used in the gravity inversion.

and the interpretation of the distribution of oceanic lithosphere, the distal extent of thinned continental crust and OCTZ structure, are not significantly dependent on the break-up age or ocean isochrons. However, it is important that the lithosphere thermal gravity-anomaly correction is included in the gravity inversion. The effect of omitting the lithosphere thermal gravity-anomaly correction is shown in Figure 5g and h, and results in a significant increase in predicted crustal thickness and a decrease in lithosphere thinning factor. Within the oceanic domain of the SCS, omitting the lithosphere thermal gravity-anomaly correction results in crustal thicknesses in the range 10–15 km (rather than *c.* 7 km) and thinning factors of *c.* 0.7 rather than 1.0 as expected for oceanic lithosphere.

Sensitivity tests have also been carried out for other parameters used in the gravity inversion: reference Moho depth, sediment thickness and the parameterization of decompression melting. A reference Moho depth of 40 km has been used to produce the gravity-inversion results shown in Figures 3 and 4, and is preferred. The effect of decreasing the reference Moho depth used in the gravity inversion to 37.5 km (Fig. 6a and b) decreases the predicted crustal thickness and increases the lithosphere thinning; increasing the reference Moho depth to 42.5 km (Fig. 6e and f) has the opposite effect. These variations in reference Moho depth do not, however, significantly affect the overall interpretation of the distribution of oceanic crust, the distal extent of continental crust and the regional OCTZ structure. A detailed explanation of the reference Moho depth and its importance in determining crustal thickness from gravity inversion is given in Cowie *et al.* (2015).

The effect of omitting sediment thickness from the gravity inversion has a more significant effect (Fig. 7c and d), resulting in an increase in predicted crustal thickness and a decrease in thinning factor. The overall shape of the predicted oceanic domain in the SCS does not change much (except in the NE of the SCS). However, the OCT structure on both the northern and southern margins does

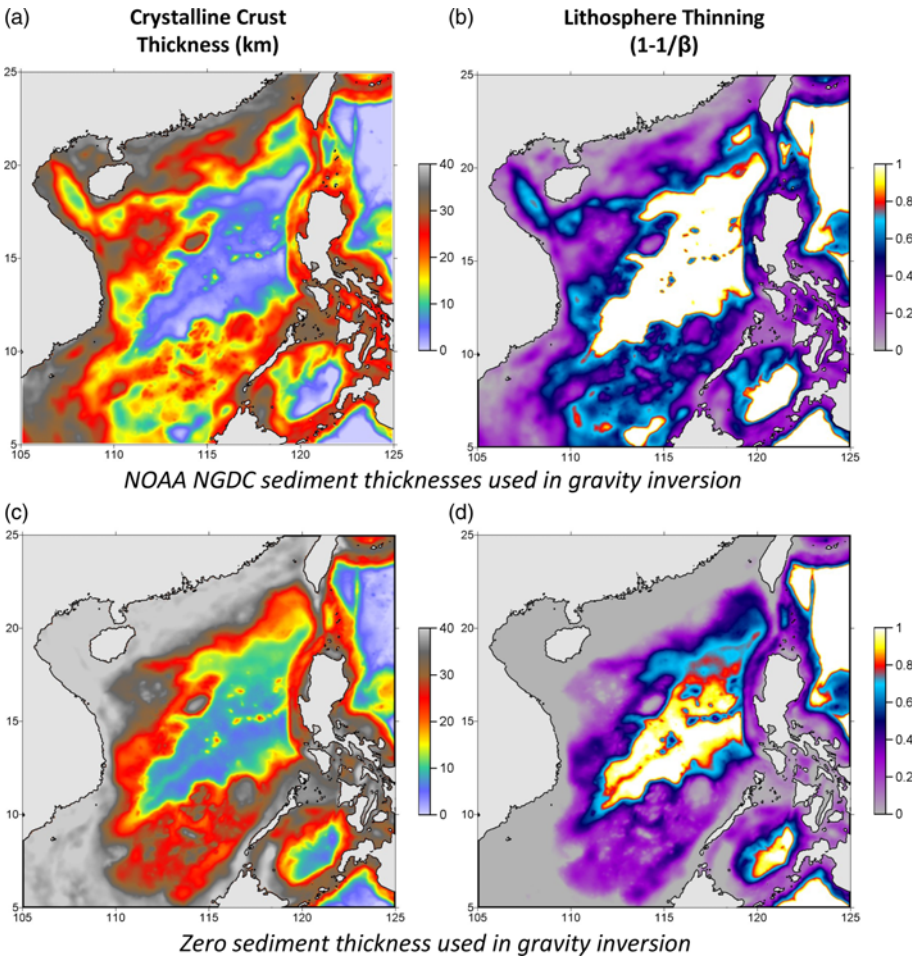

Fig. 7. Sensitivity of crustal thickness and continental lithosphere thinning determined from gravity inversion to sediment thickness used in the gravity inversion. (**a**) & (**b**) Using NOAA-NGDC sediment thickness. (**c**) & (**d**) Using zero-thickness sediments.

change significantly. This illustrates the importance of sediment-thickness data in the gravity inversion.

The maps shown in Figures 3 and 4 were produced using a parameterization of decompression melting which produces normal thickness (7 km) oceanic crust. The effect of decreasing decompression melting, corresponding to magma-poor break-up and seafloor spreading, is to decrease the predicted lithosphere thinning from gravity inversion (Fig. 8b) to maximum values of 0.8–0.9. These values are less than the value of 1.0 that corresponds to oceanic lithosphere. Thinning factors of 0.9 could be indicative of serpentinized exhumed mantle (see Cowie *et al.* 2015 for a detailed discussion); however, in the absence of other evidence, we prefer the normal decompression melt solution (Figs. 3, 4 and 8d). The effect of increasing the strength of decompression melting to that corresponding to a magma-rich break-up producing a 10 km-thick oceanic crust is to increase the predicted lithosphere thinning factor from gravity inversion (Fig. 8f), which slightly enlarges the predicted oceanic domain within the SCS; however, we do not see evidence to support magma-rich decompression melting. It is worth noting that the effect of changing the magnitude of magmatic addition within the gravity inversion has only a very minor effect on the thickness of predicted crustal thickness.

Comparison of gravity-inversion results using 3D public-domain sediment-thickness data with sediment thickness from a 2D regional seismic profile crossing the SCS

The 3D gravity-inversion mapping of Moho depth, crustal thickness and continental lithosphere thinning described in the previous section uses public-domain sediment-thickness data (Divins 2003). We compare these results with gravity-inversion and subsidence-analysis predictions using more detailed sediment-thickness data obtained from a BGR (Bundesanstalt für Geowissenschaften und Rohstoffe) regional seismic reflection section crossing the SCS from the Pearl River Mouth Basin (PRMB) to the conjugate Palawan margin. As well as comparing Moho depth, we use the sediment thickness from the seismic reflection data to determine continental lithosphere thinning profiles using both gravity inversion and subsidence analysis. Moho depth and continental lithosphere thinning profiles produced by different input data and analytical methods are then compared for validation purposes. The BGR seismic cross-section in two-way travel time (TWT) is shown in Figure 9. The seismic line location is shown on Figure 1.

Moho depth and crustal thickness from gravity inversion using sediment thickness derived from the BGR seismic-reflection data are shown in Figure 10a. As well as showing the thinning of crystalline crust on both the PRMB and Palawan continental margins, the cross-section also shows crust 15–20 km thick under the NE continuation of the Macclesfield Bank. The Macclesfield Bank has significantly less sediment on top of basement due to isolation from sediment sources and catchment areas to its immediate north and south. The oceanic crustal thickness of the SCS is typical of average oceanic crust predominantly varying between 5 and 7 km. The thickness of oceanic crust is thinnest adjacent to the OCTZ offshore Palawan.

Figure 10a also shows crust thicker than normal oceanic crust associated with seamounts in the region of the fossil ocean ridge along the central axis of the SCS. We believe that this thicker crust is real and not an artefact of the gravity-inversion method. It would imply that the cessation of seafloor spreading in the eastern SCS was associated with excess magmatism; similar excess magmatism is

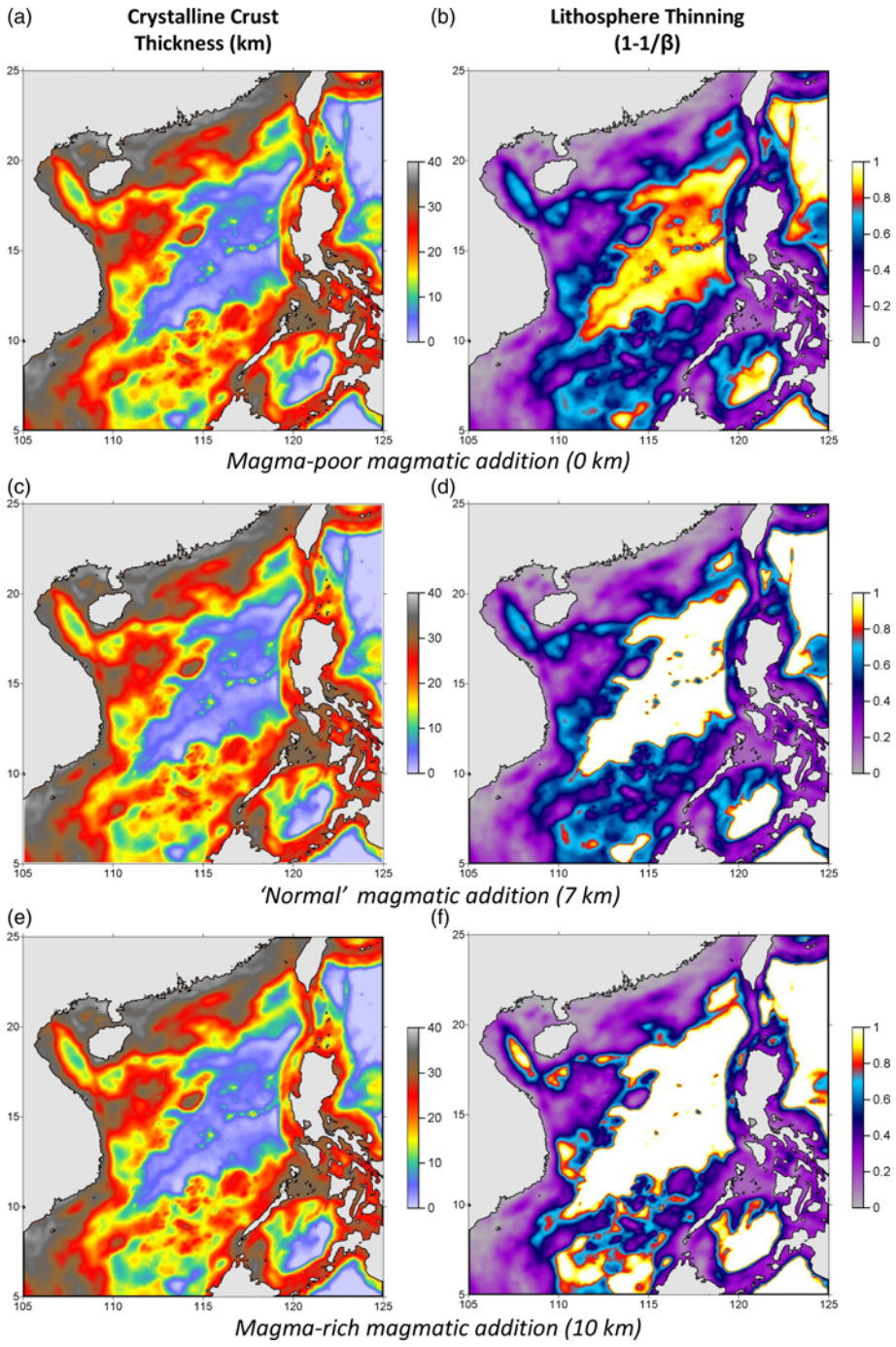

Fig. 8. Sensitivity of crustal thickness and continental lithosphere thinning determined from gravity inversion to magmatic addition from decompression melting. (**a**) & (**b**) Using magma-poor magmatic addition (0 km). (**c**) & (**d**) Using normal magmatic addition (7 km). (**e**) & (**f**) Using magma-rich magmatic addition (10 km).

seen on the fossil spreading axis of the proto-oceanic Gop Rift, west of India (Corfield *et al.* 2010).

For comparison, Moho depth from gravity inversion using the public-domain sediment-thickness data is shown in Figure 10b. The cross-section produced using public-domain sediments is generally similar to that produced using the reflection-derived sediment-thickness data but has less resolution. The greatest thickness difference is about 2 km in the southern SCS. Profiles of continental lithosphere thinning produced by gravity inversion assuming normal decompression melting, and using both BGR and NOAA public-domain sediment thicknesses, are shown in Figure 7c and are also similar.

Continental lithosphere thinning has also been determined for the BGR regional seismic profile using subsidence analysis (Fig. 11). The subsidence analysis uses flexural backstripping and decompaction plus palaeobathymetry assumptions to derive continental lithosphere thinning using a modified McKenzie (1978) pure-shear model that includes a subsidence correction for magmatic addition from decompression melting. Water-loaded subsidence of top pre-rift is assumed to be generated by the combination of initial synrift lithosphere subsidence (including crustal thinning) and post-rift thermal subsidence: that is, $S_i + S_t$, where S_i is synrift subsidence and S_t is post-rift (post-break-up) thermal subsidence. The methodology for converting water-loaded subsidence into continental thinning factors is described in Roberts *et al.* (2013) and Cowie *et al.* (2015). Global eustasy for sea-level change since the onset of rifting (Haq *et al.* 1987; Harland *et al.* 1989) has been included when determining the water-loaded subsidence. A correction for mantle dynamic topography variation with time has not been applied.

The determination of the water-loaded subsidence requires a palaeobathymetry indicator within the stratigraphy. At the time of the onset of rifting, the margins were in a coastal marine setting, as determined from seismic facies and confirmed by Ocean Drilling

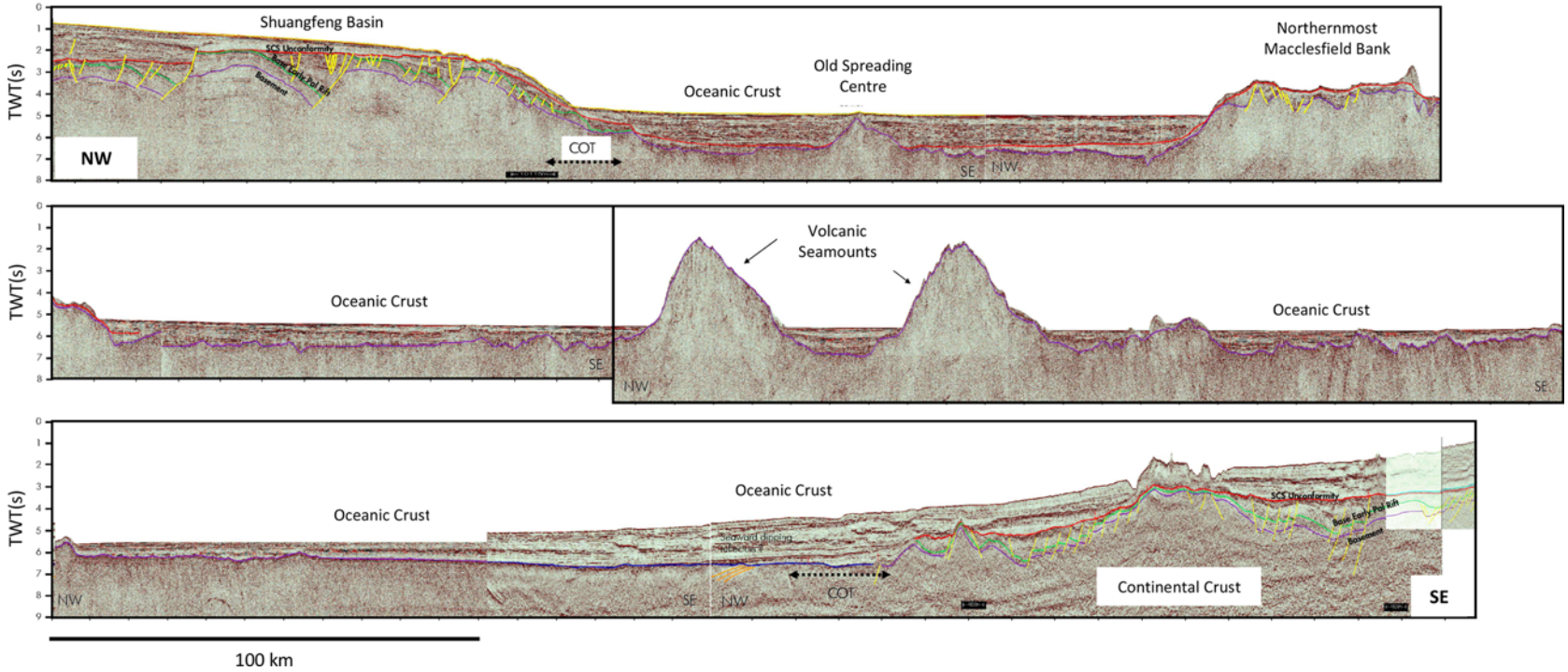

Fig. 9. The composite BGR seismic reflection line (line 1 in Fig. 1a) from offshore China to Palawan. The seismic line traverses the Pearl River Mouth Basin, the Shuangfeng Basin, the northernmost extent of the Macclesfield Bank and the oceanic crust of the South China Sea. The red line is interpreted as the base of the post-rift sediments. COT, ocean–continent transition.

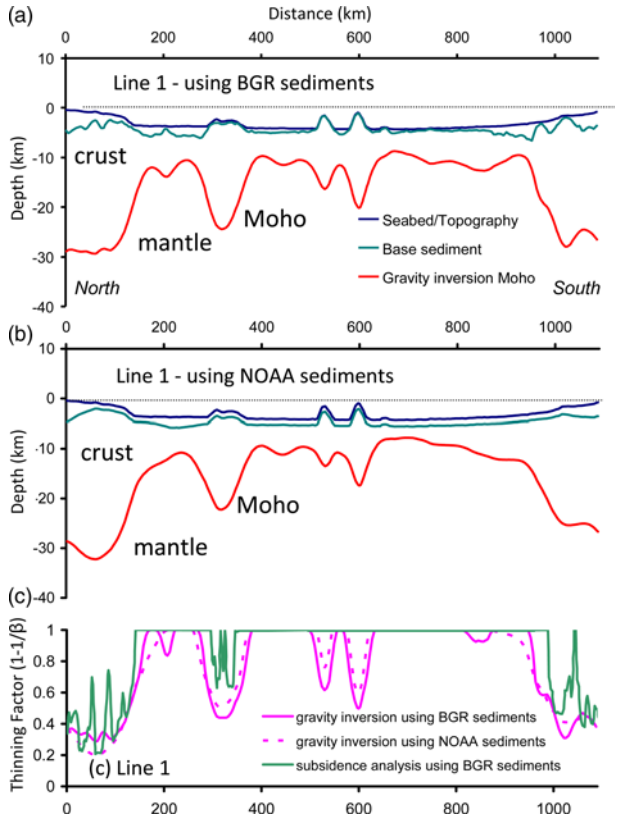

Fig. 10. Crustal cross-sections with Moho from gravity-anomaly inversion along line 1. (**a**) Crustal cross-section using sediments from the BGR seismic reflection profile. (**b**) Crustal cross-section using NOAA sediment-thickness data. (**c**) Comparison of continental thinning ($1-1/\beta$) along line 1 determined from gravity inversion using the BGR and NOAA sediment thickness and from subsidence analysis. Line locations are shown in Figure 1.

Program (ODP) Site 1148. Within the flexural backstripping modelling, the post-, syn- and pre-rift sediment sequences were assigned densities and compaction decay constants depending on the average lithology in that sequence. The post-rift sediment sequence is predominantly shale, the synrift sediments are a mixture of sands and shales, and the pre-rift is a mixture of conglomeratic sandstones with intervals of siltstone including some coaly fragments. The regional flexural response to the unloading of sediments is controlled by an effective elastic thickness (T_e). Braitenberg *et al.* (2006) reported that T_e ranges from 2 to 4 km in the region of the SCS. We have used a T_e value of 3 km in the flexural backstripping of this profile to calculate water-loaded subsidence. Sensitivity tests to T_e (0–10 km) have been carried out and show that its value is not critical.

While rifting would have taken place for several millions of years prior to the continental break-up, initial seafloor spreading is assumed to have occurred at *c.* 33 Ma in the eastern SCS (Barckhausen & Roeser 2004). The age of the break-up unconformity of 33 Ma has been recently confirmed at the Chinese margin based on results of IODP drilling (Li *et al.* 2014) and we use this age in the subsidence analysis.

Continental lithosphere thinning determined from subsidence analysis for the reflection seismic profile is shown in Figure 11d. The subsidence correction for magmatic addition assumes a decompression melt parameterization that generates a normal 7 km thickness oceanic crust. Sensitivities to break-up age are shown and the predicted differences are deemed insignificant. Thinning at or near 1 in Figure 11d is interpreted as showing oceanic crust between the Macclesfield Bank and offshore Palawan, and between the Macclesfield Bank and offshore China (as also shown in Fig. 4b).

In Figure 10c, continental lithosphere thinning determined from subsidence analysis is compared with lithosphere thinning determined from gravity inversion using both BGR seismic-reflection and NOAA public-domain sediment-thickness data. The two different methods (gravity inversion and subsidence analysis) give a very similar distribution of lithosphere thinning even though they use different methodologies and observational data. They both show the same pattern of lithosphere thinning across the PRMB and Palawan margins and the Macclesfield Bank, and similar values, at or near 1, for the regions of oceanic crust.

It is noteworthy that both the gravity-inversion and subsidence-analysis methods identify the oceanic seamounts at the failed seafloor-spreading centre on the central axis of the SCS. The thinning factors predicted by both methods over the seamounts have values much less than 1, as would be expected for normal oceanic crust and lithosphere. This is because a normal decompression melt parameterization has been used which is set to predict a 7 km-thick oceanic crust. Failure to account for the melt production above 7 km thickness results in a thinning factor of less than 1. Nonetheless, we believe that the axial seafloor-spreading zone of the zone of the SCS is underlain by oceanic crust.

Discussion and summary

Crustal basement thickness and continental lithosphere thinning maps have been determined using 3D gravity inversion for the SCS (Figs 3 and 4b), and are used to show the regional distribution of oceanic crust, the distal extent of continental crust and OCTZ structure. Additional regional tectonic information can be gained by examining the free-air gravity-anomaly and magnetic-anomaly maps. The free-air gravity anomaly (Fig. 2a) clearly shows the fossil ocean ridge along the axis of the SCS, as well as continental shelf breaks. The change in the character of the free-air gravity anomaly from NE to SW along the fossil ocean ridge may correspond to a decrease in magmatic addition and the frequency of seamounts. The magnetic-anomaly map (Fig. 2d) shows a strong NE–SW-trending anomaly pattern within the ocean crust and parallel to the fossil ocean ridge axis. The magnetic anomalies also show an east–west pattern within continental margin crust.

Figure 12 shows a shaded relief free-air gravity anomaly superimposed onto gravity-derived crustal thickness and continental lithosphere thinning maps determined using gravity inversion. Oceanic crust within the SCS can be clearly identified by both the distribution of thin crust (Figs 3 and 12a) and where lithosphere thinning factors are equal to, or near to, 1 (Figs 4b and 12b). Within the oceanic domain, the extinct seafloor-spreading axis can be seen striking NE–SW and faint traces of an oceanic transform fault striking approximately north–south. The extinct seafloor-spreading centre shows slightly thicker than normal oceanic crust associated with seamounts in the eastern part of the SCS. This thicker oceanic crust at the fossil seafloor-spreading centre is also shown on the regional BGR seismic-reflection line (Figure 10). The superimposed shaded-relief free-air gravity anomaly shows different structural trends within oceanic crust compared with the thinned continental margin crust. Within the thinned continental crust of the margin, a strong structural trend striking ENE–WSW can be seen both on the northern margin of the SCS and in the Dangerous Grounds region. We interpret this trend as being associated with synrift deformation of continental crust in the OCTZ. These structural trends correspond to the orientation of the salient of oceanic crust between the PRMB margin and the Macclesfield Bank in the north of the SCS. The north–south oceanic fracture zone at 116° E seen in Figure 12 may be inherited from a large strike-slip system that limited the western extent of early seafloor spreading in

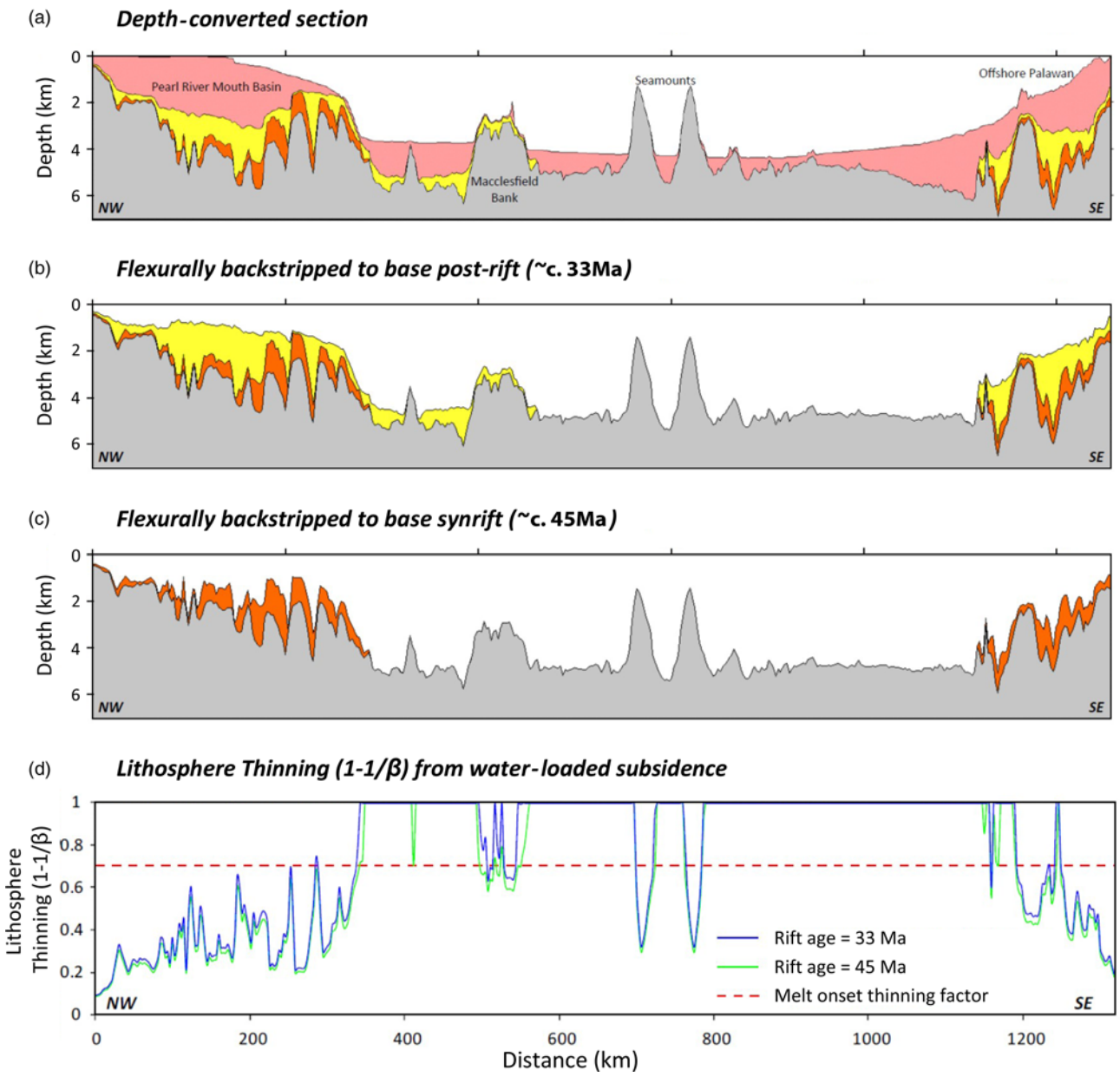

Fig. 11. (**a**) Depth-converted cross-section along the BGR line (line 1) showing post-rift, synrift and pre-rift sediment sequences. Post-rift sediments are pink, synrift sediments are yellow and pre-rift sediments are orange. (**b**) Cross-section after the removal of the post-rift sequence by flexural backstripping and decompaction of the pre-rift and synrift sediments. Flexural isostatic response of the lithosphere uses $T_e = 3$ km. (**c**) Cross-section after the removal of post-rift and synrift sequences by flexural backstripping and decompaction of the pre-rift sediments. (**d**) Lithosphere thinning ($1-1/\beta$) determined from water-loaded subsidence of top pre-rift obtained from flexural backstripping and decompaction. Sensitivities to rifting ages of 45 and 33 Ma are shown. The red line indicates the critical thinning factor of 0.7 (corresponding to β value of *c*. 3) for the onset of normal decompression melting. Note that the distance origin of this profile differs from that of Figures 9 and 10.

the SCS and which continued southwards bounding the eastern limit of the Dangerous Grounds region. Figure 12 also shows that the southern margin of the SCS is segmented by strike-slip faults leading to a 'staircase'-like OCTZ geometry.

The superposition of shaded relief magnetic anomalies (using the EMAG2-v3 compilation: Meyer *et al.* 2017) onto crustal thickness and continental lithosphere thinning maps from gravity inversion is shown in Figure 13. Within the oceanic domain, two distinct trends of magnetic anomalies can be seen: one with a NE–SW strike adjacent and parallel to the extinct seafloor-spreading axis; and the other in the eastern SCS with a more ENE–WSW trend located closer to the distal extent of continental crust on the Chinese and Palawan margins. These two trends can be seen in the ocean isochron maps of Barckhausen *et al.* (2014), and suggest that seafloor spreading occurred first in the eastern SCS and had a ENE–WSW strike compared with the younger seafloor spreading, which propagated further west and had a more NE–SW strike. The strike of the older seafloor-spreading axis in the eastern SCS corresponds to the ENE–WSW structural trends seen on the northern margin of the SCS and in the Dangerous Grounds region (Fig. 12).

A set of crustal cross-sections, with Moho from gravity inversion, is shown in Figure 14. These lines, orientated in the dip direction, cross the SCS from the NW China–Vietnam margins to the SE Malaysia–Brunei–Philippines margins and show the variation in OCTZ structure and ocean-basin width. Figure 14 shows that the SCS conjugate margins are highly asymmetrical, and have several notable features such as the Macclesfield Bank, Xisha Trough, Reed Bank and Dangerous Grounds (Figs 1 and 3). The OCTZ structure and relationship of the conjugate margins within the SCS is complex

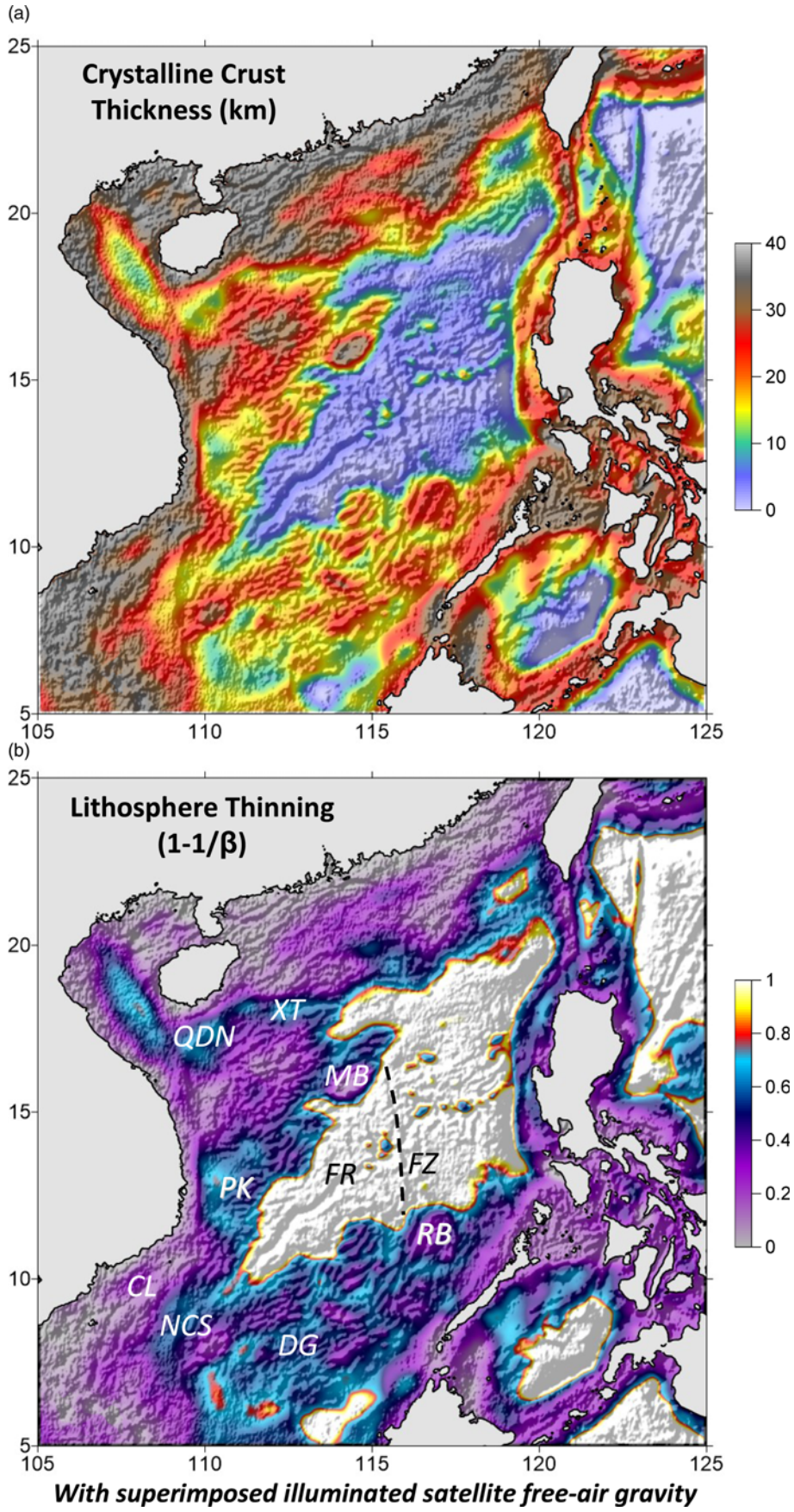

Fig. 12. (**a**) Crustal basement thickness from gravity inversion with superimposed shaded relief free-air gravity anomaly. (**b**) Continental lithosphere thinning from gravity inversion with superimposed shaded relief free-air gravity anomaly. Features referenced in the text: FR, Fossil Ridge; FZ, 116° E Fracture Zone; MB, Macclesfield Bank; MT, Manila Trench; PRMB, Pearl River Mouth Basin; RB, Reed Bank; SB, Shuangfeng Basin; XT, Xisha Trough.

partly because of rift and spreading ridge jumps which led to the formation of the isolated blocks of continental crust such as the Macclesfield and Reed banks (Cullen *et al.* 2010). The Reed Bank, once part of the same continental block as the Macclesfield Bank, is predicted to have a crustal thickness of 20–25 km, which is similar to the present-day crustal thickness of the Macclesfield Bank.

The two rift and continental break-up events either side of the Macclesfield Bank result in the higher thinning factor values

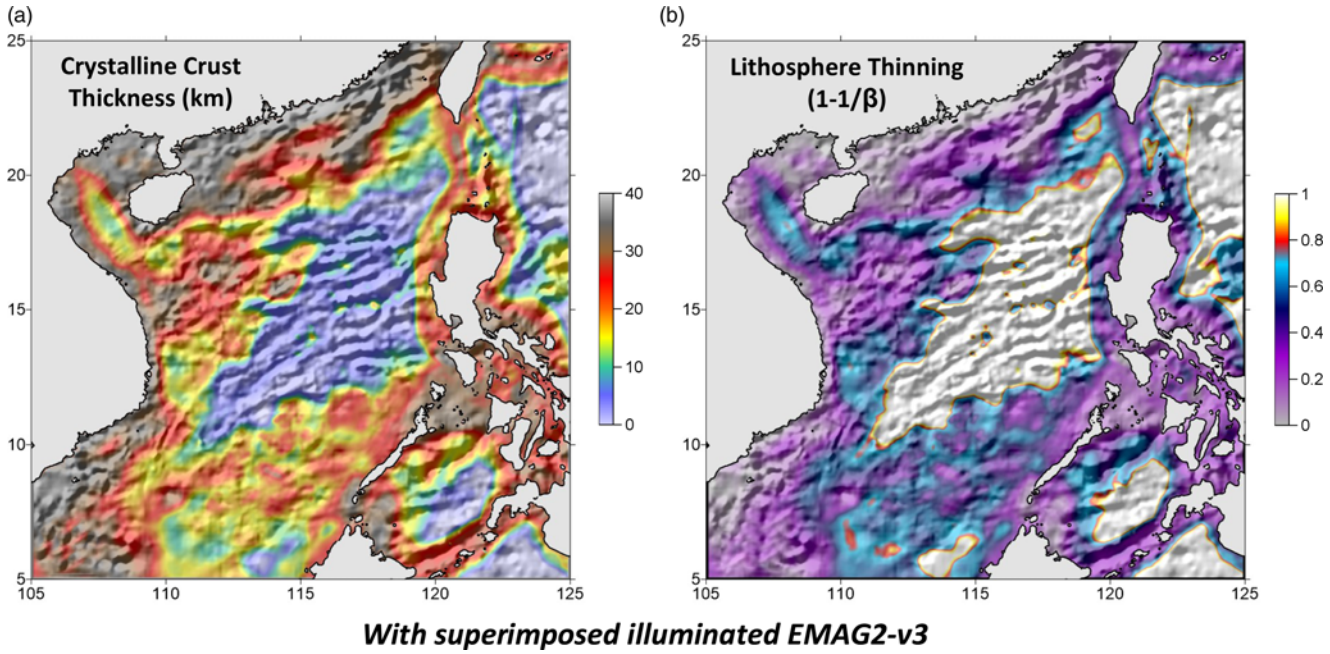

Fig. 13. (**a**) Crustal thickness from gravity inversion with superimposed shaded relief magnetic anomaly (EMAG2-v3). (**b**) Continental lithosphere thinning from gravity inversion with superimposed shaded relief magnetic anomaly.

measured beneath the Macclesfield Bank compared with offshore China or offshore Palawan (Figs 4b and 10c). Earlier studies by Clift & Lin (2001) and Sun *et al.* (2009) have suggested that on the northern margin of the SCS, in the Pearl River Mouth Basin and South China slope, the extension continued for *c.* 5–8 myr after the onset of seafloor spreading. Thus, the onset of seafloor spreading and the generation of oceanic crust may not here correspond to the immediate cessation of continental margin rifting. The initiation of seafloor spreading following the ridge jump at around 24 Ma to the south of the Macclesfield Bank has had the largest impact on the present-day geography of the SCS region. The continental margin offshore China, incorporating the Pearl River Mouth Basin, appears to be significantly wider than the offshore Palawan margin; however, this may be due to the modification of the Palawan margin by compressional tectonics in the Miocene and subduction of some SCS crust.

The Dangerous Grounds, west of the Reed Bank, are also predicted to consist of thinned continental crust. Crustal thicknesses from gravity inversion show that the southern margin of the SCS in the west consists of fragmented blocks of thinned continental crust separated by thinner regions that have undergone higher degrees of stretching and thinning. Crust in this region has been thinned to a higher degree than the Reed Bank and the crustal thickness here is predicted to be significantly less, generally ranging from 10 to 20 km thick, which is in accordance with refraction seismic modelling (Pichot *et al.* 2014). In contrast to the relatively narrow Palawan margin of the SCS, the southern SCS margin further west shows thinned continental crust which gets progressively wider on the Dangerous Grounds margin, as seen in the crustal thickness and continental lithosphere thinning determined from gravity inversion (Figs 3, 4b and 12). This raises the question of whether the Dangerous Grounds should be interpreted as a broad region of necked continental crust within the OCTZ. The Dangerous Grounds, which have a crustal thickness of 10–20 km, would appear to correspond to a very wide OCTZ.

In the western segment of the SCS only one continental break-up event occurred, as the early break-up event to the north of the Macclesfield Bank did not propagate as far westwards. The ridge jump, at 24 Ma coincides with a noticeable change in the spreading azimuth of the SCS. This suggests that the ridge jump is a response driven by changes in the regional stress field (Cullen *et al.* 2010). The change in location of the spreading centre does not alone account for the formation of the Dangerous Grounds and the Baram Basin. An important and not yet resolved issue is deconvolving the signal of regional Eocene rifting of the Dangerous Grounds and Luconia from the younger opening of the SCS (Cullen 2014). However, most of the rifting associated with the formation of the Dangerous Grounds is believed to predate the opening of the SCS (Thies *et al.* 2005; Cullen 2014).

The thinning factor profiles determined for crust and lithosphere using gravity inversion and subsidence analysis are in reasonable agreement (Fig. 10c), A detailed fault analysis is beyond the scope of this paper; however, a cursory fault-heave summation gives a β stretching factor of 1.2 or less for the PRMB and Palawan margins. Assuming depth–uniform thinning, this β stretching factor converts to a thinning factor of less than 0.2 to allow a direct comparison with whole crustal and whole lithospheric thinning factors. In contrast, lithosphere thinning from subsidence analysis and gravity inversion for the PRMB and Palawan margins is *c.* 0.4. Davis & Kusznir (2004) reported a similar thinning discrepancy between fault-heave summation and crustal thinning for the offshore China margin within the OCTZ (but converging to similar thinning values inboard in the Pearl River Basin: see Su *et al.* 1989; Clift & Lin 2001). One explanation for this thinning discrepancy may be that fault-heave summation underestimates stretching and thinning because of the limitations of fault-heave measurement using seismic reflection imaging (Reston 2007, 2010). An alternative explanation is that the SCS continental margin lithosphere has experienced depth-dependent lithosphere stretching and thinning (Roberts *et al.* 1997; Driscoll & Karner 1998; Davis & Kusznir 2004; Kusznir & Karner 2007). Clift *et al.* (2002) and Ding *et al.* (2013) studied three transects in the Dangerous Grounds and estimated the extension due to the faulting. Their results demonstrated a distinct difference between whole crustal thinning and fault-derived extension. This might imply a preferential extension of the ductile portions of the crust under the Dangerous Grounds (Clift & Lin 2001). However, Franke *et al.* (2014) provided evidence for local polyphase faulting during

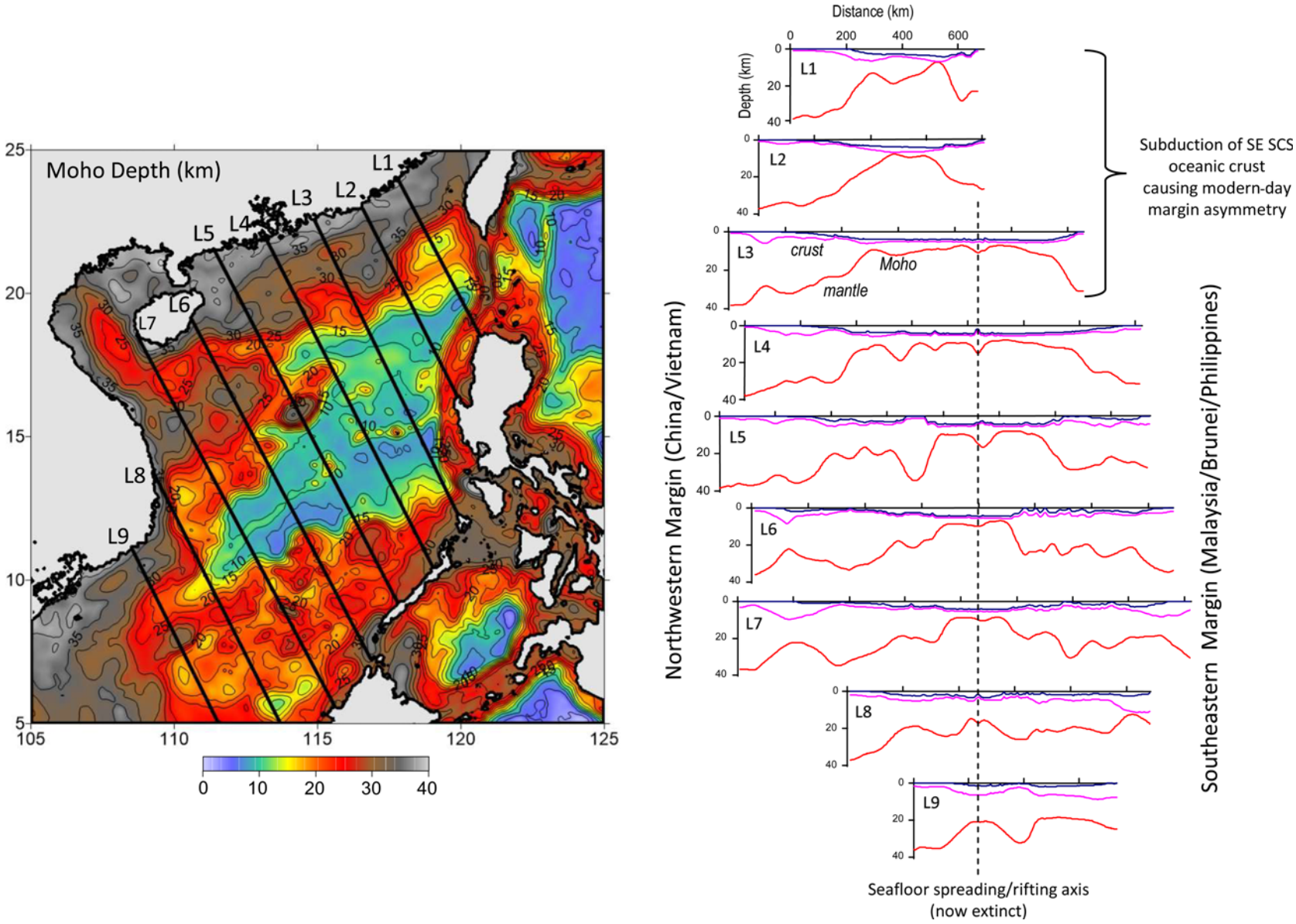

Fig. 14. Crustal cross-sections with Moho depth from gravity inversion showing the along-strike variations of OCTZ structure and ocean-basin width for the South China Sea. Line locations are superimposed on a map of Moho depth determined using gravity inversion.

rifting – a process that would contribute to an underestimation of fault-controlled extension.

Geophysical inversion of satellite-derived free-air gravity-anomaly data incorporating a lithosphere thermal gravity-anomaly correction provides a useful and reliable methodology for mapping global crustal thickness in the marine domain (Chappell & Kusznir 2008). The resulting maps of crustal thickness and continental lithosphere thinning factor may be used to determine OCTZ structure: that is, the location and extent of necked continental crust and hyperextended crust, and the distribution of oceanic lithosphere and continental fragments. Crustal cross-sections using Moho depth from gravity inversion also allow OCTZ structure and magmatic type (i.e. magma-poor, 'normal' or magma-rich) to be determined. Using crustal thickness and continental lithosphere thinning factor maps with a superimposed shaded-relief free-air gravity anomaly, we can improve the determination of rift orientation and seafloor-spreading trajectory during ocean-basin formation and pre-break-up rifted margin conjugacy.

Acknowledgements We thank Andy Alvey and Alan Roberts of Badley Geoscience for discussions and also reviewers for their helpful and constructive comments.

Funding S.G. was funded by the MM2 industry consortium.

References

Alvey, A., Gaina, C., Kusznir, N. & Torsvik, T. 2008. Integrated crustal thickness mapping and plate reconstructions for the high Arctic. *Earth and Planetary Science Letters*, **274**, 310–321.

Arfai, J., Franke, D. *et al.* 2011. Geological evolution of the West Luzon Basin (South China Sea, Philippines). *Marine Geophysical Research*, **32**, 349–362.

Barckhausen, U. & Roeser, H.A. 2004. Seafloor spreading anomalies in the South China Sea revisited. *In*: Clift, P., Kuhnt, W., Wang, P. & Hayes, D. (eds) *Continent–Ocean Interactions within East Asian Marginal Seas*. American Geophysical Union, Geophysical Monographs, **149**, 121–125.

Barckhausen, U., Engels, M., Franke, D., Ladage, S. & Pubellier, M. 2014. Evolution of the South China Sea: Revised ages for breakup and seafloor spreading. *Marine and Petroleum Geology*, **58**, 599–611.

Braitenberg, C., Wienecke, S. & Wang, Y. 2006. Basement structures from satellite-derived gravity field: South China Sea ridge. *Journal of Geophysical Research: Solid Earth*, **111**, B05407, https://doi.org/10.1029/2005JB003938

Briais, A., Patriat, P. & Tapponnier, P. 1993. Updated interpretation of magnetic-anomalies and sea-floor spreading stages in the South China Sea – Implications for the Tertiary tectonics of Southeast-Asia. *Journal of Geophysical Research: Solid Earth*, **98**, 6299–6328.

Cameselle, A.L., Ranero, C.R., Franke, D. & Barckhausen, U. 2017. The continent–ocean transition on the northwestern South China Sea. *Basin Research*, **29**, 73–95.

Chappell, A.R. & Kusznir, N.J. 2008. Three-dimensional gravity inversion for Moho depth at rifted continental margins incorporating a lithosphere thermal gravity anomaly correction. *Geophysical Journal International*, **174**, 1–13.

Clift, P. & Lin, J. & ODP Leg 184 Scientific Party. 2001. Patterns of extension and magmatism along the continent–ocean boundary, South China margin. *In*: Wilson, R.C.L., Whitmarsh, R.B., Taylor, B. & Froitzheim, N. (eds) *Non-Volcanic Rifting of Continental Margins: A Comparison of Evidence from Land and Sea*. Geological Society, London, Special Publications, **187**, 489–510, https://doi.org/10.1144/GSL.SP.2001.187.01.24

Clift, P., Lin, J. & Barckhausen, U. 2002. Evidence of low flexural rigidity and low viscosity lower continental crust during continental break-up in the South China Sea. *Marine and Petroleum Geology*, **19**, 951–970.

Corfield, R.I., Carmichael, S., Bennett, J., Akhter, S., Fatimi, N. & Craig, T. 2010. Variability in the crustal structure of the West Indian Continental Margin in the Northern Arabian Sea. *Petroleum Geoscience*, **16**, 257–265, https://doi.org/10.1144/1354-079309-902

Cowie, L., Kusznir, N. & Manatschal, G. 2015. Determining the COB location along the Iberian margin and Galicia Bank from gravity anomaly inversion, residual depth anomaly and subsidence analysis. *Geophysical Journal International*, **203**, 1355–1372.

Cullen, A. 2014. Nature and significance of the West Baram and Tinjar lines, NW Borneo. *Marine and Petroleum Geology*, **51**, 197–209.

Cullen, A., Reemst, P., Henstra, G., Gozzard, S. & Ray, A. 2010. Rifting of the South China Sea: new perspectives. *Petroleum Geoscience*, **16**, 273–282, https://doi.org/10.1144/1354-079309-908

Davis, M. & Kusznir, N.J. 2004. Depth-dependent lithospheric stretching at rifted continental margins. *In*: Karner, G.D. (ed.) *Proceedings of NSF Rifted Margins Theoretical Institute*. Columbia University Press, New York, 92–136.

Ding, W. & Li, J. 2016. Propagated rifting in the Southwest Sub-basin, South China Sea: Insights from analogue modelling. *Journal of Geodynamics*, **100**, 71–86.

Ding, W., Franke, D., Li, J. & Steuer, S. 2013. Seismic stratigraphy and tectonic structure from a composite multi-channel seismic profile across the entire Dangerous Grounds, South China Sea. *Tectonophysics*, **582**, 162–176.

Divins, D.L. 2003. *Total Sediment Thickness of the World's Oceans and Marginal Seas*. NOAA National Geophysical Data Center, Boulder, CO.

Driscoll, N.W. & Karner, G.D. 1998. Lower crustal extension across the Northern Carnarvon basin, Australia: Evidence for an eastward dipping detachment. *Journal of Geophysical Research*, **103**, 4975–4991.

Expedition 349 Scientists 2014. South China Sea tectonics: Opening of the South China Sea and its implications for southeast Asian tectonics, climates, and deep mantle processes since the late Mesozoic, *International Ocean Discovery Program Preliminary Report*, 349, https://doi.org/10.14379/iodp.pr.349.2014

Franke, D., Barckhausen, U., Heyde, I., Tingay, M. & Ramli, N. 2008. Seismic images of a collision zone offshore NW Sabah/Borneo. *Marine and Petroleum Geology*, **25**, 606–624.

Franke, D., Barckhausen, U. *et al.* 2011. The continent–ocean transition at the southeastern margin of the South China Sea. *Marine and Petroleum Geology*, **28**, 1187–1204.

Franke, D., Savva, D., Pubellier, M., Steuer, S., Mouly, B. & Auxietre, J. 2014. The final rifting evolution in the South China Sea. *Marine and Petroleum Geology*, **58**, 704–720.

Gabo, J.A.S., Dimalanta, C.B., Asio, M.G.S., Queano, K.L., Yumul, G.P. Jr. & Imai, A. 2009. Geology and geochemistry of the clastic sequences from Northwestern Panay (Philippines): Implications for provenance and geotectonic setting. *Tectonophysics*, **479**, 111–119.

Gao, J., Wu, S., McIntosh, K., Mi, L., Liu, Z. & Spence, G. 2016. Crustal structure and extension mode in the northwestern margin of the South China Sea. *Geochememistry, Geophysics, Geosystems*, **17**, 2143–2167, https://doi.org/10.1002/2016GC006247

Greenhalgh, E.E. & Kusznir, N.J. 2007. Evidence for thin oceanic crust on the extinct Aegir Ridge, Norwegian Basin, NE Atlantic derived from satellite gravity inversion. *Geophysical Research Letters*, **34**, L06305, https://doi.org/10.1029/2007GL029440

Hall, R. 2002. Cenozoic geological and plate tectonic evolution of SE Asia and the SW Pacific: computer-based reconstructions, model and animations. *Journal of Asian Earth Sciences*, **20**, 353–431.

Haq, B.U., Hardenbol, J. & Vail, P.R. 1987. Chronology of fluctuating sea levels since the Triassic. *Science*, **235**, 1156–1167.

Harland, W.B., Armstrong, R.L., Cox, A.V., Craig, L.E., Smith, A.G. & Smith, D.G. 1989. *A Geologic Timescale 1989*. Cambridge University Press, Cambridge.

Hinz, K., Block, M., Kudrass, H.R. & Meyer, H. 1994. Structural elements of the Sulu Sea, Philippines. *AAPG Bulletin*, **78**, 1146.

Hutchison, C.S. & Vijayan, V.R. 2010. What are the Spratly Islands? *Journal of Asian Earth Sciences*, **39**, 371–385.

Koppers, A.A.P. 2014. On the $_{39}Ar/_{40}Ar$ dating of low-potassium ocean crust basalt from IODP expedition 349, South China Sea. AGU Fall meeting 2014, T31E-03.

Kudrass, H.R., Wiedicke, M. & Cepek, P. 1985. Mesozoic and Cenozoic rocks dredged from the South China Sea and their significance for plate-tectonic reconstructions. *Marine and Petroleum Geology*, **3**, 19–30.

Kusznir, N. & Karner, G.D. 2007. Continental lithospheric thinning and breakup in response to upwelling divergent mantle flow: application to the Woodlark, Newfoundland and Iberia margins. *In*: Karner, G.D., Manatschal, G. & Pinheiro, L.M. (eds) *Imaging, Mapping and Modelling Continental Lithosphere Extension and Breakup*. Geological Society, London, Special Publications, **282**, 389–419, https://doi.org/10.1144/SP282.16

Li, C.F., Xu, X. *et al.* 2014. Ages and magnetic structures of the South China Sea constrained by deep tow magnetic surveys and IODP Expedition. *Geochemistry, Geophysics, Geosystems*, **15**, 4958–4983, https://doi.org/10.1002/2014GC005567

Liu, W.-N., Li, C.-F., Li, J., Fairhead, D. & Zhou, Z. 2014. Deep structures of the Palawan and Sulu Sea and their implications for opening of the South China Sea. *Marine and Petroleum Geology*, **58**, 721–735.

McIntosh, K., Lavier, L., van Avendonk, H. & Liu, C. 2014. Crustal structure and inferred rifting processes in the northeast South China Sea. *Marine and Petroleum Geology*, **58**, 612–626.

McKenzie, D. 1978. Some remarks on the development of sedimentary basins. *Earth and Planetary Science Letters*, **40**, 25–32.

Meyer, B., Chulliat, A. & Saltus, R. 2017. Derivation and error analysis of the earth magnetic anomaly grid at 2 arc min resolution version 3 (EMAG2v3). *Geochemistry, Geophysics, Geosystems*, **18**, 4522–4537.

Milliman, J.D. & Meade, R.H. 1983. World-wide delivery of river sediment to the oceans. *Journal of Geology*, **91**, 1–21.

Mitchell, A.H.G. & Leach, T.M. 1991. *Epithermal Gold in the Philippines: Island Arc Metallogenesis. Geothermal Systems and Geology*. Academic Press, London.

Mohn, G., Manatschal, G., Beltrando, M., Masini, E. & Kusznir, N. 2012. Necking of continental crust in magma-poor rifted margins: Evidence from the fossil Alpine Tethys margins. *Tectonics*, **31**, TC1012, https://doi.org/10.1029/2011TC002961

Parker, R.L. 1972. The rapid calculation of potential anomalies. *Geophysical Journal of the Royal Astronomical Society*, **31**, 447–455.

Pichot, T., Delescluse, M. *et al.* 2014. Deep crustal structure of the conjugate margins of the SW South China Sea from wide-angle refraction seismic data. *Marine and Petroleum Geology*, **58**, 627–643.

Pigott, J.D. & Ru, K. 1994. Basin superposition on the northern margin of the South China Sea. *Tectonophysics*, **235**, 27–50.

Reston, T. 2007. Extension discrepancy at North Atlantic nonvolcanic rifted margins: Depth-dependent stretching or unrecognized faulting? *Geology*, **35**, 367–370.

Reston, T. 2010. The opening of the central segment of the South Atlantic: symmetry and the extension discrepancy. *Petroleum Geoscience*, **16**, 199–206, https://doi.org/10.1144/1354-079309-907

Roberts, A.M., Lundin, E.R. & Kusznir, N.J. 1997. Subsidence of the Vøring Basin and the influence of the Atlantic continental margin. *Journal of the Geological Society, London*, **154**, 551–557, https://doi.org/10.1144/gsjgs.154.3.0551

Roberts, A., Kusznir, N., Corfield, R., Thompson, M. & Woodfine, R. 2013. Integrated tectonic basin modelling as an aid to understanding deep-water rifted continental margin structure and location. *Petroleum Geoscience*, **19**, 65–88, https://doi.org/10.1144/petgeo2011-046

Sandwell, D.T. & Smith, W.H.F. 1997. Marine gravity anomaly from Geosat and ERS 1 satellite altimetry. *Journal of Geophysical Research: Solid Earth*, **102**, 10 039–10 054.

Schlüter, H.U., Hinz, K. & Block, M. 1996. Tectono-stratigraphic terranes and detachment faulting of the South China Sea and Sulu Sea. *Marine Geology*, **130**, 39–78.

Smith, W.H.F. & Sandwell, D.T. 1997. Global sea floor topography from satellite altimetry and ship depth soundings. *Science*, **277**, 1956–1962.

Su, D., White, N. & McKenzie, D. 1989. Extension and subsidence of the Pearl River Mouth Basin, northern South China Sea. *Basin Research*, **2**, 205–222, https://doi.org/10.1111/j.1365-2117.1989.tb00036.x

Sun, Z., Zhong, Z. *et al.* 2009. 3D analogue modeling of the South China Sea: A discussion on breakup pattern. *Journal of Asian Earth Sciences*, **34**, 544–556.

Taylor, B. & Hayes, D.E. 1980. The tectonic evolution of the South China Basin. *In*: Hayes, D.E. (ed.) *The Tectonic and Geologic Evolution of Southeast Asian Seas and Islands*. American Geophysical Union, Geophysical Monographs, **23**, 89–104.

Thies, K., Mansor, A., Hamdon, M., Bishkel, R., Boyer, J. & Tearpock, D. 2005. Structural and stratigraphic development of extensional basins: A case study offshore deepwater Sarawak and northwest Sabah, Malaysia. AAPG Search and Discovery Article #10103, AAPG Annual Convention, June 19–22, 2005, Calgary, Alberta, Canada.

Tugend, J., Manatschal, G., Kusznir, N. & Masini, E. 2014. Characterizing and identifying structural domains at rifted continental margins: application to the Bay of Biscay margins and its Western Pyrenean fossil remnants. *In*: Gibson, G.M., Roure, F. & Manatschal, G. (eds) *Sedimentary Basins and Crustal Processes at Continental Margins: From Modern Hyper-extended Margins to Deformed Ancient Analogues*. Geological Society, London, Special Publications, **413**, 171–203, https://doi.org/10.1144/SP413.3

Wan, K., Xia, S., Cao, J., Sun, J. & Xu, H. 2017. Deep seismic structure of the northeastern South China Sea: Origin of a high-velocity layer in the lower crust. *Journal of Geophysical Research: Solid Earth*, **122**, 2831–2858.

White, R. & McKenzie, D. 1989. Magmatism at rift zones: the generation of volcanic continental margins and flood basalts. *Journal of Geophysical Research*, **94**, 7685–7729.

Yumul, G.P., Dimalata, C.B., Marquez, E.J. & Quean, K.L. 2009. Onland signatures of the Palawan microcontinental block and Philippine mobile belt. *Journal of Asian Earth Sciences*, **34**, 610–623.

Zhao, F., Alves, T.M. *et al.* 2016. Prolonged post-rift magmatism on highly extended crust of divergent continental margins (Baiyun Sag, South China Sea). *Earth and Planetary Science Letters*, **445**, 79–91.